4-21-2022

Naphthalene-functionalized resorcinarene as selective, fluorescent self-quenching sensor for kynurenic acid†

Anna Karle
Oakland University, 146 Library Drive, Rochester, Michigan

Kwaku Twum
Oakland University, 146 Library Drive, Rochester, Michigan

Noorhan Sabbagh
Oakland University, 146 Library Drive, Rochester, Michigan

Alise Haddad
Oakland University, 146 Library Drive, Rochester, Michigan

S. Maryamdokht Taimoory
Department of Chemistry and Biochemistry, University of Windsor,

See next page for additional authors

ARTICLE

Naphthalene-Functionalized Resorcinarene as Selective, Fluorescent Self-Quenching Sensor for Kynurenic Acid

Received 00th January 20xx,
Accepted 00th January 20xx

DOI: 10.1039/x0xx00000x

Anna Karle[a], Kwaku Twum[a], Noorhan Sabbagh[a], Alise Haddad[a], S. Maryamdokht Taimoory [b,c], Małgorzata M. Szczęśniak[a], Evan Trivedi[a], John F. Trant[b], Ngong Kodiah Beyeh[a]*

Kynurenic acid is a by-product of tryptophan metabolism in humans, with abnormal levels indicative of disease. There is a need for water-soluble receptors that selectively bind kynurenic acid, allowing for detection and quantification. We report here the high-affinity binding of kynurenic acid in aqueous media to a resorcinarene salt receptor decorated with four flexible naphthalene groups at the upper rim. Experimental results from ^{1}H NMR, isothermal titration calorimetry, and electronic absorption and fluorescence spectroscopies all support high-affinity binding and selectivity for kynurenic acid over tryptophan. The measured binding constant (K = 1.46±0.21×10^5 M^{-1}) is one order of magnitude larger than that observed with other resorcinarene receptors. The present host-guest system can be employed for sensory recognition of kynurenic acid. Computational studies reveal the key role of a seriers of cooperative attractive intra- and inter-molecular interactions contributes to an optimal binding process in this system.

Introduction

Tryptophan (Trp), besides its role in proteins, is of particular interest due to its autofluorescence,[1–3] as an antidepressant,[4] as an appetite suppressant,[5] and as a sleep aid.[6] It is also notable for being the precursor of 5-hydroxytryptophan (5HT), and consequently serotonin. However, only 1% of dietary Trp is converted to 5HT, with over 95% metabolized to Kynurenic acid (KynA).[7,8] KynA is a known antagonist of excitatory amino acid receptors, and as such, is a biomarker for excitotoxicity and several neurogenerative diseases.[8] Low levels of KynA in the brain present a confounding risk factor in major depressive disorders associated with worsening neurological disease.[9] KynA serum levels have been used by clinicians to track both the progression of seizures and the therapeutic outcome of antiepileptic drugs.[8,10]

However, these tools are limited. For example, y-globulin stabilized nanogold clusters have been used for sensing kynurenine in phosphate buffer.[11] In another report, biological samples of Trp and KynA were precipitated in methanol before using liquid chromatography-tandem mass spectrometry (LC-MS) for quantification and detection.[10] Zinc(II) complexes of KynA have also been used for laser-induced fluorescence detection in microdialysate samples.[12] Most current approaches require elaborate sample preparation to separate KynA from Trp using tedious techniques.[13] There is a need for a water-soluble organic receptor that can selectively bind KynA allowing for simple detection and/or quantification without additional sample preparation or complex instrumentation.

'Green' sensory recognition elements are beneficial for their high efficiency and simple application.[14–18] Organic receptors for physiologically-relevant bioanalytes are designed to be functional and selective in water, physiological buffers, or mixed solvent systems. In organic supramolecular chemistry, this is usually achieved by carefully functionalizing the periphery with water-soluble groups while designing the core pocket/groups to be selective for the bio-analyte of interest. Resorcinarenes are aromatic receptors with shallow cavities and are often used for molecular recognition.[19,20] Modifications can be made at either the upper or lower rim of resorcinarenes, introducing unique properties for applications in crystal engineering,[21–23] solution-phase host-guest chemistry,[24–27] and gas-phase complexation.[28–30] *N*-Alkyl ammonium resorcinarene halides (NARXs) are hydrogen-bonded analogs of cavitands possessing deeper cavities suitable for host-guest processes. By decorating the NARXs with different appendages, they can be used as suitable receptors for specific bio analytes *via* weak interactions.[31] The strength and reversibility of non-covalent interactions in aqueous media, coupled with the confined cavities of macrocyclic receptors and specific properties of peripheral functional groups could be tuned to provide selective binging for KynA over Trp. In this contribution, we report a NARX receptor decorated with four flexible naphthalene groups with high affinity for KynA and selectivity for this metabolite over Trp in aqueous media. This has been established through the synergistic application of ^{1}H NMR spectroscopy, isothermal titration calorimetry (ITC), fluorescence, UV spectrophotometry, and computational analysis.

[a] Oakland University, 146 Library Drive, Rochester, Michigan, 48309-4479, USA.
[b] Department of Chemistry and Biochemistry, University of Windsor, 401 Sunset Avenue, Windsor, ON, N9B 3P4, Canada.
[c] Department of Chemistry, University of Michigan, 930 N. University Ave, 2811 Ann Arbor, MI 48019, USA.

Electronic Supplementary Information (ESI) available: [details of any supplementary information available should be included here]. See DOI: 10.1039/x0xx00000x

Results and discussion

Three previously reported resorcinarenes (**1-3**) bearing either a sulfonate group (**1**), a flexible ammonium n-propanol (**2**), or a rigid ammonium n-cyclohexyl (**3**) upper rim functionality were synthesized according to reported procedures (Figure 1).[31–33] Our new NARX receptor (**4**), with four fluorescent naphthyl groups with large surface areas for aromatic interactions, was prepared by treating the basic resorcinarenes[34] with 1-naphthyl amine in the presence of excess formaldehyde. Cleavage of the resulting 6-membered tetrabenzoxazine under reflux with concentrated HCl delivers NARCl **4** (Figure 1, Figure S1).[31,35] The receptors were screened for their selective binding of KynA over Trp. Due to the limited solubility of KynA, we used a mixed solvent system of H_2O/DMSO (v.v. 70%/30%).

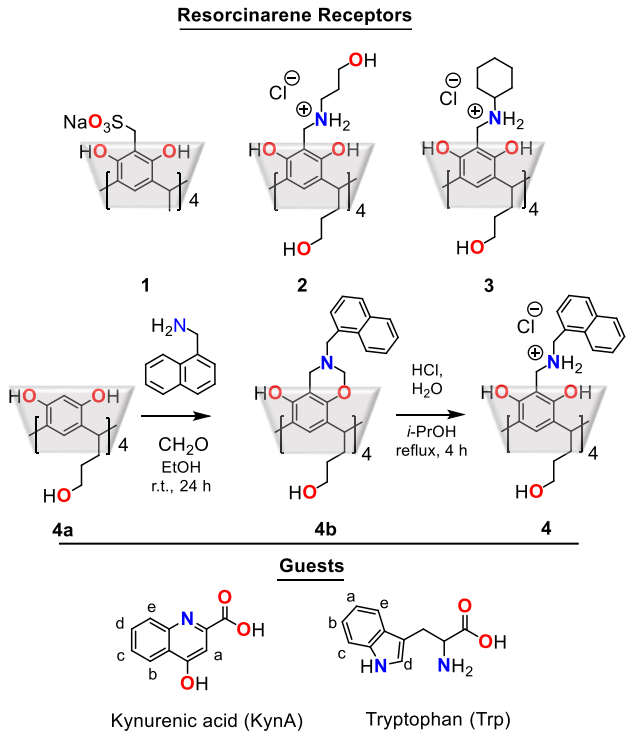

Figure 1: Resorcinarene-based receptors (**1-4**) and guests, kynurenic acid (KynA) and tryptophan (Trp).

NMR Spectroscopy

^{1}H NMR spectroscopy was used for screening the affinity of the receptors **1-4** for KynA (Figure 2, Figure S4 – S6). This was done by monitoring the complexation-induced chemical shift changes of the host-guest complex compared to the pure host and guest. Guest complexation in the resorcinarene cavity is typically indicated by shielding and broadening of the guests' ^{1}H NMR signals.[36] This qualitative measure of binding was only observed for receptor **4**, indicating the importance of naphthalene functionality in the upper rim of the resorcinarene. Taking the interaction between KynA and Trp vs receptor **4** as an example, an upfield shift (0.06 ppm) of the KynA signals implies complexation. In analogous experiments with Trp, changes in chemical shift were negligible, suggesting weak in-cavity interaction with the receptor **4** (Figure 2).

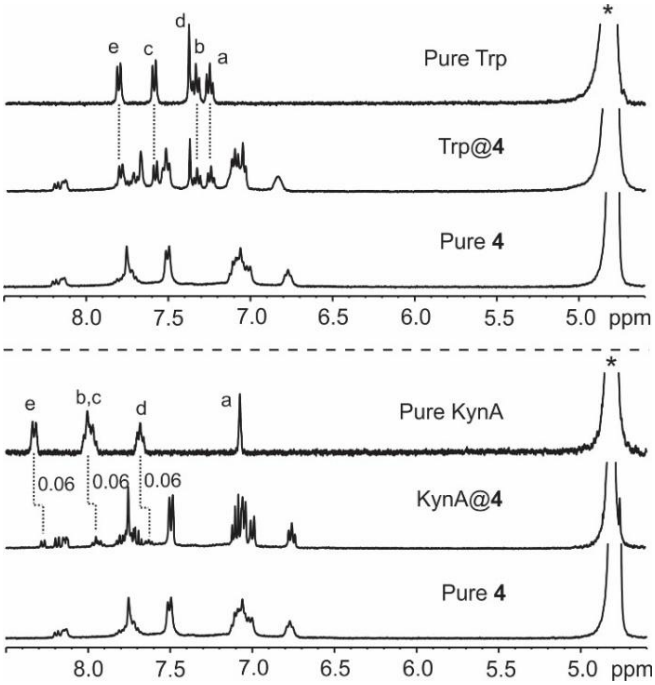

Figure 2: ^{1}H NMR showing receptor **4** (1 mM), complexation of KynA (Bottom) and Trp (Top) with receptor **4** at 1:1 molar ratio in 70%D_2O, 30% D_6[DMSO] at 298 K. Star (*) represents D_2O signal used as calibrant.

Considering the small ^{1}H NMR shift changes, typical for these resorcinarene salts receptors,[ref] we did some 2D NMR experiments to further illuminate the binding process. First, we monitored complexation between receptor **4** and the guests Trp and KynA through 2D nuclear Overhauser enhancement spectroscopy (NOESY). The spectra confirmed that the aromatic protons of the benzyl arm of the receptor **4** and the Trp are in close proximity (Figure 3a). We could not confirm this spatial relationship for KynA. However, 2D NOESY NMR spectroscopy is insufficiently diagnostic to confirm host-guest interactions unambiguously, so we turned to Diffusion Ordered Spectroscopy (DOSY) NMR experiments to further probe the host guest interactions. DOSY can identify host guest assemblies in solution by monitoring their diffusion coefficients since it depends on a molecules molecular weight, solvodynamic radius, and interactions.[ref] We observed a diffusion coefficient of 1.23×10^{-9} m^2s^{-1} and 1.29×10^{-9} m^2s^{-1} for isolated receptor **4** and KynA respectively (Figure S7). An equimolar mixture of **4** and KynA substantially reduces these values to 0.59×10^{-9} m^2s^{-1} and 0.81×10^{-9} m^2s^{-1} respectively, indicating slower movement, and a larger hydrodynamic radius (Figure 3b). This strongly supports our contention that they interact in solution.

ARTICLE

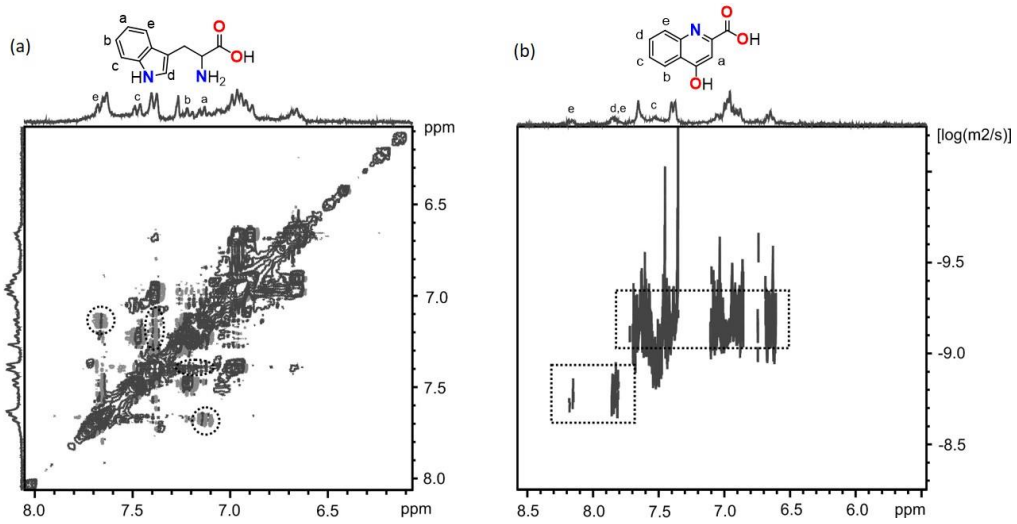

Figure 3: (a) 2D NOESY NMR spectra of 1mM solution of receptor **4** and Trp 70%D_2O, 30% D_6[DMSO] at 298 K. (b) 2D DOSY NMR spectra of receptor **4** and KynA in 70%D_2O, 30% D_6[DMSO] at 298 K.

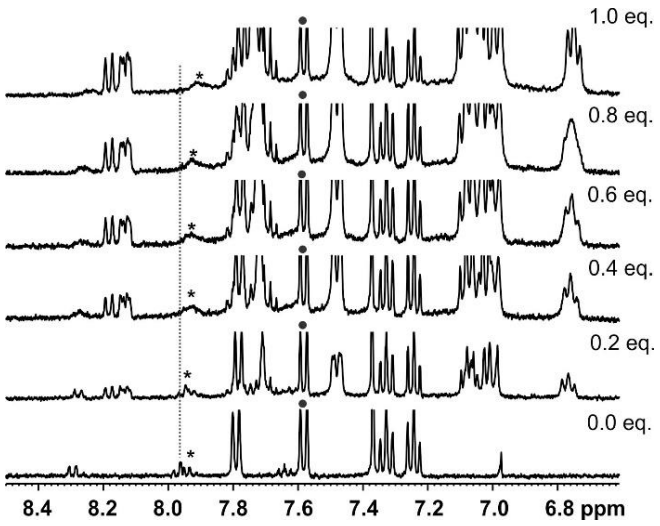

Figure 4: Competitive NMR titration of different equivalence of receptor **4** into a 1:8 mixture of KynA and Trp. Signal (*) tracks KynA protons, signal (●) tracks Trp protons.

Next, we assessed the selectivity of receptor **4** for KynA over Trp through a series of ^{1}H NMR competition experiments. In the first experiment, we titrated different equivalents (0.2 – 1.0) of receptor **4** into a 1:8 mixture of KynA and Trp. Despite the considerable excess of Trp, a complete preference for interacting with KynA over Trp was observed. Upon addition of the receptor **4**, an apparent broadening and up field shifts of the KynA signals are observed (Figure 4), while no changes were made to the Trp signals. To further illustrate the selectivity for KynA over Trp, we carried out two extra experiments. In the first, we a prepared 1:1 mixture of receptor **4** and Trp. To this solution, we added one equivalent of KynA and monitored the changes in the resonances (Figure Sxx). The results show clear changes for Kyna indicating that it is bound and is the preferred guest. In the subsequent experiment, we a prepared 1:1 mixture of receptor **4** and KynA. To this solution, we added one equivalent of Trp and monitor the shift changes (Figure 5). No changes to the KynA signals was observed, suggesting that its chemical environment remained identical; suggesting that Trp cannot displace KynA from **4**.

Isothermal Titration Calorimetry (ITC)

ITC was used to determine the thermodynamic parameters (K, ΔH, ΔS, and ΔG) of receptor-guest interactions in both H_2O/DMSO (70/30, v/v) and in Tris buffer/DMSO (70/30, v/v) (Figure S9). The DMSO cosolvent was necessary to ensure the complete dissolution of the KynA and receptors **3** and **4** at the required concentrations. All data were fitted to a one-site binding model except for KynA@**2**. In that case, the hydroxyl end groups of the upper rim could be responsible for secondary binding through hydrogen bonds. All the other receptors, lacking this functionalization, were readily fitted to a one-site binding model. Negative ΔG values reveal binding to be spontaneous at 298 K. The negative ΔH, and TΔS values indicate the complexation to be enthalpy driven, but entropy compensated. The positive ΔH and TΔS value for the first binding process in KynA@**2** indicate that the process is entropy (desolvation) driven.

The interaction between receptor **4** and KynA reveals a remarkably high binding constant (Ka = 1.46±0.21×10^5 M^{-1} in the water mixture, and Ka = 7.08±0.65×10^4 M^{-1} in the buffer mixture, Table 1). The large surface area of the aromatic

naphthyl groups is instrumental to driving this affinity for KynA, demonstrating the strength of hydrophobic π-π aromatic interactions even in protic solvents. The weakest binding was observed for the receptors not possessing any aromatic functionality at the upper rim (Table 1). This highlights the importance of aromatic interactions. The binding constant for the interaction between **4** and Trp was substantially lower, again highlighting the preference for KynA. The ITC traces of all the titrations are provided as Supporting Information (Figure S9). It is important to note that in any real application, the concentration would be far lower and would be conducted in water. In that case, the binding constant is likely even higher as DMSO acts as a competing solvent, inhibiting the interaction.

Table 1: Thermodynamic binding parameters of formed complexes between the receptors and the guests by ITC.

Complex	*Ka* (× 10^4) M^{-1}	*ΔH* kcal/mol	*TΔS* kcal/mol	*ΔG* kcal/mol
KynA@**1**	0.12±0.01	-175±6.60	-170.46	-4.54
KynA@**2**	0.075±0.02	9.1±0.01	12.96	-3.86
	1.47±0.66	-12.1±3.43	-6.47	-5.63
KynA@**3**	0.36±0.096	-16.5±1.6	-11.65	-4.85
KynA@**4**	14.60±2.15	-19.4±0.35	-12.37	-7.03
KynA@**4***	7.08±0.65	-12.4±0.21	-5.75	-6.65
Trp@**4***	0.39±0.05	-41.32±2.2	-36.36	-4.96

ITC was done in H_2O/DMSO (70%/30%) at 298 K. *ITC was done in pH 7.4 Tris buffer (10mM) /DMSO (70%/30%) at 298 K.

Fluorescence Spectroscopy

Standard resorcinarenes are weakly fluorescent.[37] However, the naphthalene functionalization of **4** provides a strong fluorescence signal that is quenched in the presence of the KynA guest (Figure S10). KynA is also fluorescent, and its inherent fluorescence is also quenched in the presence of increasing concentrations of receptor **4 (**Figure 5). The first introduction of receptor **4** changes the microenvironment around the fluorophore to create a new emission peak around 470nm. It is noteworthy that the 350 nm excitation wavelength employed in this titration does not result in the fluorescence of free receptor **4** (Figure S11).

$$\lambda_{max} = 400\text{nm}$$

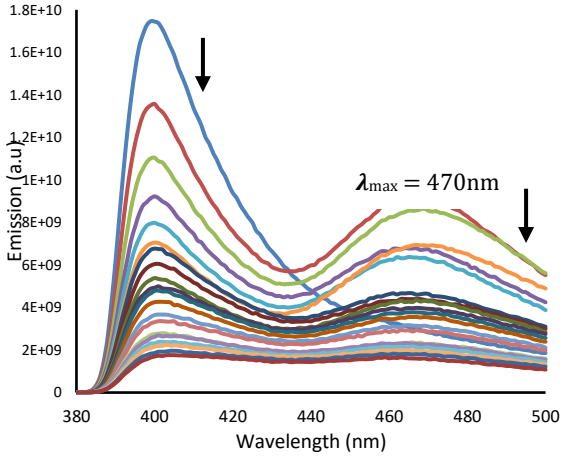

Figure 5: Steady state emission spectra (λ_{exc}=350nm) of KynA in H_2O/DMSO (70%/30%, 298 K) at different equivalents of receptor **4**: 0.00, 0.30, 0.60, 0.90, 1.19, 1.49, 1.78, 2.08, 2.37, 2.66, 2.96, 3.44, 3.92, 4.40, 5.83, 6.76, 7.69, 8.61 and 9.52 equivalents.

We hypothesize that KynA and receptor **4** form a stable, non-fluorescent ground state complex that is responsible for their mutual fluorescent quenching. To probe the mechanism of fluorescent quenching, we plotted the Stern-Volmer relationship (equation 1) for the kinetics of fluorescence intramolecular deactivation.[38–41] F and Fo are the fluorescence intensity in the presence and absence of receptor **4** respectively. [Q] refers to the concentration of receptor **4** as the 'quencher'. A linear curve would indicate that only one type of quenching from the complex formation is occurring.[42] However, a positive curvature (Figure S12a) suggests that both quenching mechanisms (collisional and static) may occur in this system.

$$\frac{Fo}{F} = 1 + K\,[Q] \qquad (1)$$

The slope of the modified Stern-Volmer plot using Equation 2 provides the static (K_s) and dynamic quenching (K_d) constants that are directly proportional to the apparent quenching constant and the rate of quenching.[43] If the two molecules interact and form a complex, quenching will take place much more often, leading to a high quenching constant.

$$\frac{Fo}{F} = (1 + Kd\,[Q])(1 + Ks[Q]) \qquad (2)$$

From the Equation 2 fit, the dynamic and static quenching constants were calculated as 11.39 and 9576, respectively (Figure S12). The high static quenching constant is indicative of a predominant non-fluorescent ground state complex between KynA and receptor **4**, however, some complexes also form in the first excited single state (dynamic quenching). Expansion of Equation 2 to the second order allows the calculation of the apparent quenching constant (K_{app}) which accounts for the upward curvature in the Stern-Volmer plot. A plot of K_{app} versus [**4**] (Figure S14) yields a straight line with a specific slope. If KynA experienced only one type of quenching, such a plot would have been a straight line parallel to the x-axis.[42]

The change in fluorescence emission intensity of the KynA upon titration with different concentrations of **4** was also analyzed. The percentage fluorescence quenching of the analyte as a function of quencher concentration was fitted using Equation 3 to obtain the dissociation constant (K_d).

$$Y = A * \frac{(X + M + K) - \left((K + X + M)^2 - (4 * M * X)\right)^{\frac{1}{2}}}{(2 * M)} \qquad (3)$$

Where A = amplitude term, X = concentration of titrant, M= concentration of fluorophore.

This model was used to fit the titration data using GraphPad Prism to obtain a K_D value of 6.35 x 10^{-5} M (K_a = 1.60 x 10^4 M^{-1}) (Figure 6). A similar titration experiment following the fluorescence signal of the naphthyl resorcinarene against titrations with different concentrations of KynA revealed a similar dissociation constant (K_D) of 6.90 x 10^{-5} M (Figure S15).

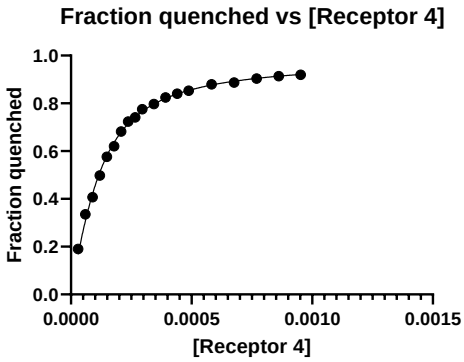

Figure 6: Fitting of percentage quenching of KynA with concentration of receptor **4**.

In comparison with the association constant obtained from ITC, we recognize that in both experimental techniques, while they nominally aim to obtain the same thermodynamic binding parameter, each method measures different things. ITC measures the transient heat of dilution changes from the complexation of the ground-state species. While the fluorescence titrations predominantly measure static quenching, they also account for the effects of collisional quenching from first excited singlet state species. This phenomenon may account for the discrepancy in binding constants obtained from the two experimental techniques.

UV-Vis Spectroscopy

That receptor **4** selectively forms host-guest complexes with KynA was also monitored using UV-Visible spectroscopic titrations. To a solution of **4** in the cell, different amounts of KynA were titrated into the solution (with care not to dilute the solution) to make effective final KynA concentrations of 0 to 0.005 M. While KynA has no absorbance beyond 360 nm, pure **4** produces a characteristic peak around 514 nm. Titration of KynA solutions into receptor **4** intensifies this characteristic signal proportional (R^2 = 0.9937) to the concentration of KynA (Figure 7). This photophysical property of receptor **4** is absent in comparable titrations with Trp (Figure S16). In addition, the absorbance signal changes as a function of guest/host equivalence were fitted to one site binding model using bindfit (Figure S17, Table S1)[ref] to obtain an affinity constant of (5.11 ± 0.35) x 10^5 M^{-1}. This agrees closely with the binding affinity obtained from ITC.

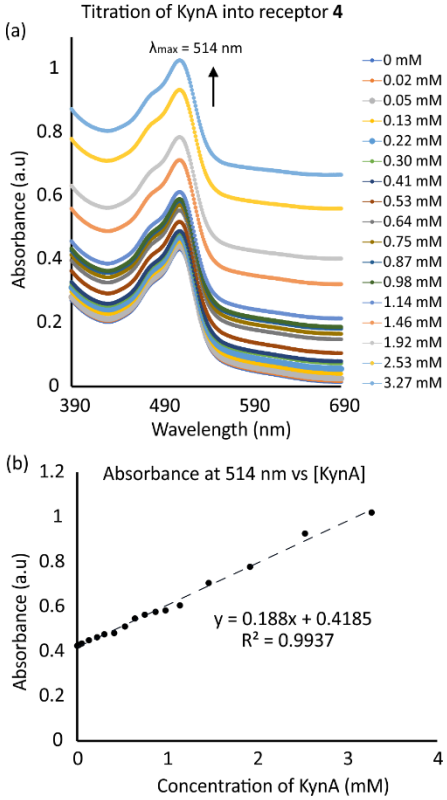

Figure 7: a) UV-Vis titration of increasing concentration of KynA (M) into a solution of receptor **4** in 50:50 H_2O/DMSO system. b) Linear response plot of absorbance at 514nm vs total KynA concentration.

Further, similar UV titrations were carried out using kynurenic acid spike human serum sample into receptor **4.** Our experiments revealed only about 10% human serum into deionized water produces a near concentration dependent increase in absorbance at 514 nm (Figure Sxx). Blank serum titration into receptor **4** produces no signal changes (Figure Sxx).

Computational Studies

The interactions between **4** and KynA and Trp were also computationally evaluated. The optimized structure of **4** is shown in Figure 8 along with its plotted electrostatic potential map. According to these calculations, **4** sits in the classic resorcinarene C_4 point group, with the bowl stabilized by a network comprising four relatively short OH---O (O---O = 2.59Å) and four NH---O (N---O = 2.83Å) hydrogen bonds. The structure is further reinforced by the four Cl^- counterions that each sit equidistant between two dangling O-H and N-H bonds. The naphthalenes decorating the rim are almost perpendicular to each other, forming the upper rim opening of ca. 8.6 Å. The electrostatic potential map shows the cavity interior to be hydrophobic. Namely, the walls show positive electrostatic potential

with the rim being even more so. Only the very bottom, aromatic part of the structure is neutral to negative.

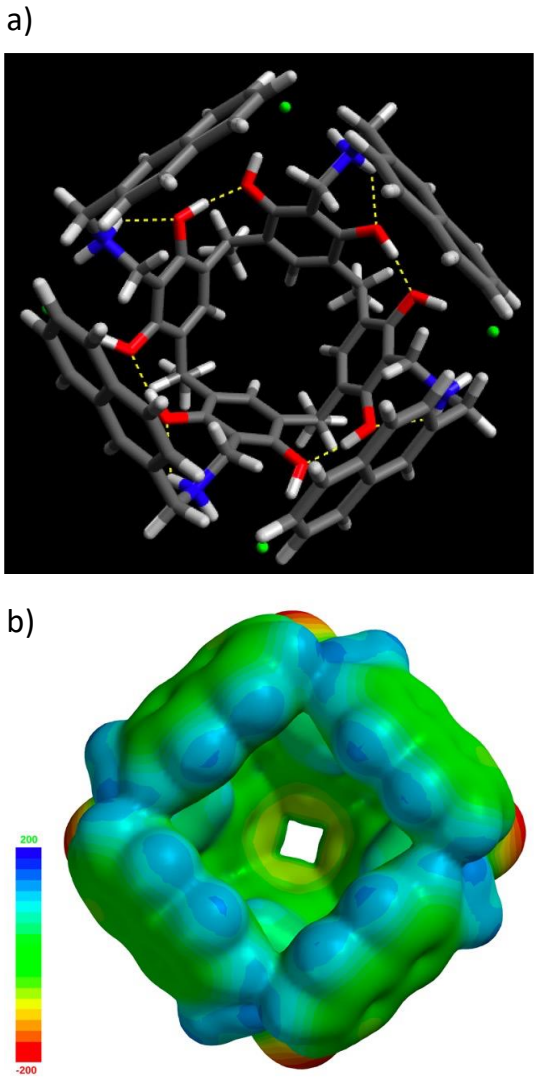

Figure 8: (a) Structure of Receptor 4; (b) Electrostatic potential mapped on the 0.002 e/au^3 isodensity surface (the scale on the left is in kJ/mol) from the B3LYP-B3 gradient optimization in def2-SVP basis set.

The structure has a considerable dipole moment of 8.3D pointing directly down into the cavity. The structural features of **4** remain essentially the same if optimized in solvent using a polarized continuum solvation model with water solvent (see Supplementary info for a brief discussion). The guest molecules are also highly polar. Trp in its more stable zwitterionic form has the dipole moment of 14D. KynA in its more stable neutral form has the dipole moment half smaller, 6.75D. Electrical considerations would thus favour the former. However, as shown below, the cavity size considerations would do the opposite. In an attempt to quantify steric effects, we employ the symmetry adapted perturbation theory (SAPT)[44] for two arbitrary configurations of the host-guest pairs. In the "outer" one the guests hover above the cavity while aligned approximately along their dipole moments axes. In the "inner" one the guests are pushed into the cavity by 3Å translation (Figure 9). The interaction energy is defined as the sum of electrostatic (elst), exchange (exch), induction (ind) and dispersion (disp) terms (Table 2). When the host and guests are far apart, the "outer" configuration, electrostatic and induction terms favour Trp over KynA because of its larger dipole moment but the dispersion terms are almost equal. This favours Trp overall.

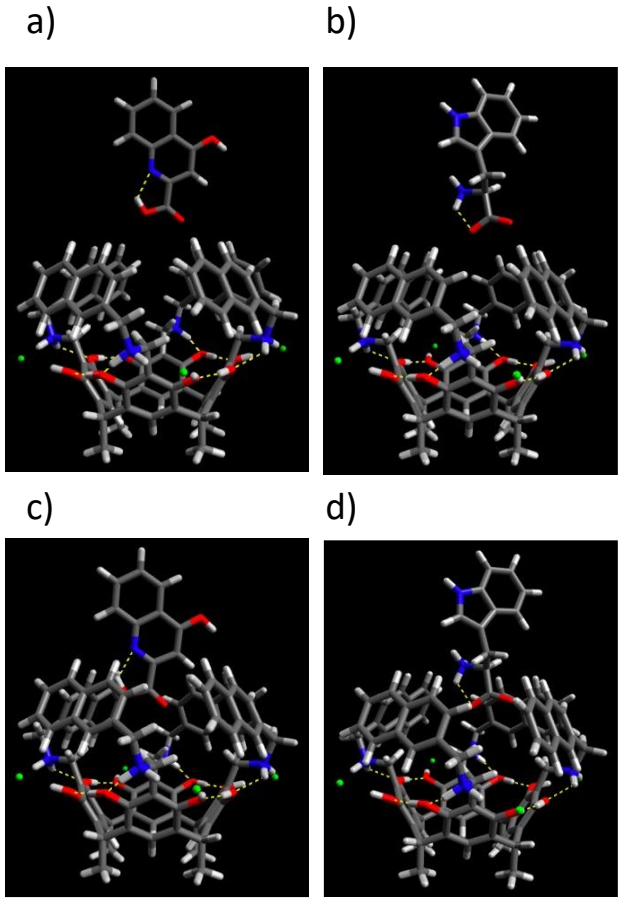

Figure 9: (top: "outer" configurations) KynA (a) and Trp (b) hover above the Receptor **4**; (down: "inner" configuration) KynA (c) and Trp (d) are lowered into **4** by 3Å along the vertical axis.

Table 2. SAPT interaction energy components for two configurations of host-guest pairs, "outer" and "inner" (see Fig. 8)

Structure	Elst	Exch	Ind	Disp	SAPT
			KynA		
outer	-1.0	0.1	-0.3	-1.8	-3.0
inner	1.8	2.3	-0.8	-7.5	-4.1
			Trp		
outer	-2.9	0.3	-1.3	-1.9	-5.7
inner	4.3	7.3	-4.4	-9.3	-2.2

When the guests insert into the host, the situation reverses. The electrostatic interaction in the "inner" configuration becomes repulsive, strongly disfavouring Trp, and so does the exchange by 5

kcal/mol. Despite the preference for Trp over KynA in the induction and (slightly) dispersion terms, the overall SAPT interaction energy favours KynA by 2 kcal/mol. It is clear that further insertion of Trp into the host will be prevented by both the exponentially rising exchange repulsion and by the unfavourable electrostatic interaction. Consequently, the entrance of Trp into the host is prevented by steric effects. As a next step we performed a gradient optimization of the KynA@**4** at the Grimme's dispersion-corrected B3LYP-D3 level of theory (Figure 10).[ref] The network of hydrogen bonds in the receptor remains intact, in fact, KynA does not seemingly hydrogen bond to the cavity interior at all. Instead, the KynA's arene is grasped in a pincer described by two facing naphthalene units. This structure implies that dispersion forces should dominate host-guest binding, precisely what the SAPT results predict (Table 3).

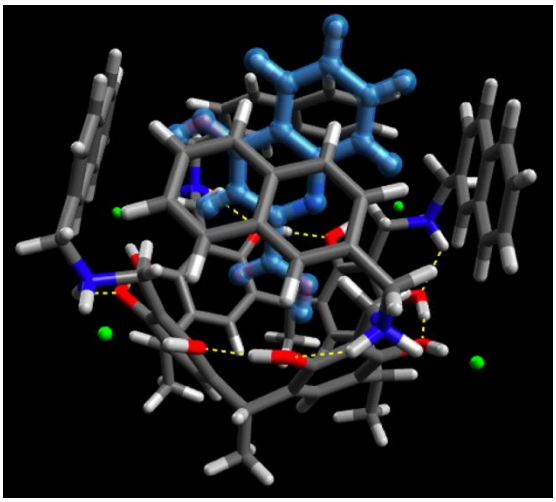

Fig. 10. Equilibrium structure of KynA@4 from B3LYP-D3 gas-phase optimization in the def2-SVP basis set. The guest molecule is shaded blue.

Table 3. SAPT components of the interaction energy between the Receptor **4** and KynA. All values in kcal/mol.

Electrostatic	Exchange	Induction	Dispersion	Overall SAPT
-18.4	40.9	-6.9	-45.1	-29.5

We conclude that the selectivity of the receptor **4** towards KynA is due to its smaller size: unlike Trp, it can fit into the narrow upper rim entrance gate of the relatively rigid host. The small size of the channel prevents Trp from entering **4**'s cavity. The structural and electronic features of the KynA@**4** complex are consistent with the findings of the NMR measurements and the fluorescent quenching observed in the experiment.

Conclusions

In summary, a naphthalene functionalized resorcinarene (**4**) is capable of high-affinity binding of kynurenic acid. The receptor, by all experimental indications, is selective for kynurenic acid over tryptophan, its parent compound. NMR spectroscopy analysis showed complexation-induced chemical shift changes not seen with the other upper rim functionalized resorcinarene receptors (**1**-**3**). Isothermal titration calorimetry showed 1:1 binding with the highest binding constant observed for the interaction between KynA and receptor **4**. The high binding was confirmed in Tris buffer at pH 7.4. Moreover, the steady-state fluorescence emission spectra show a quenching mechanism, a phenomenon most likely from a non-fluorescing ground state complex. Ground state UV absorption studies support this hypothesis. A structural explanation for this selectivity is suggested by the computational analysis. The "gateway" to the cavity is incredibly stable due to a combination of hydrogen bonds and participating counterions; this restricts the size of the opening allowing the smaller KynA in, while blocking the larger Trp. The intra-host hydrogen bonds are so strong they are not affected by the presence of the guest, and the interaction is driven almost entirely by hydrophobic collapse and dispersion interations between the π-systems of the host and guest. Considering the rising interest in supramolecular chemistry for analytical applications of host-guest complexes, the present two-component system can be exploited as a sensory recognition element for kynurenic acid. This receptor can be further employed in electrochemical, chemical, or mass sensors using a covalent or non-covalent attachment to the sensor interface.

Author Contributions

The manuscript was written and edited through the contributions of all authors. NKB, AK, KT: original concept. AK, KT, NS, AH: NMR, ITC, UV-Vis, Fluorescence. NT, MS: Computation. JT: supervised the work at University of Windsor, Canada. NKB, ET: supervised the work at Oakland, USA. All authors have approved the final version of the manuscript.

Conflicts of interest

The authors declare no conflict of interest.

Acknowledgements

The authors gratefully acknowledge financial support from Oakland University (NKB, AK, KT, NS, AH), the Oakland University Provost Graduate Research Scholarship (AK, KT), and the Natural Sciences and Engineering Research Council of Canada (2018-06338 to JFT), and the Ontario Early Researcher Award (ER18-14-114 to JFT). JFT and SMT would like to highlight that this work was made possible by the facilities of the Shared Hierarchical Academic Research Computing Network (SHARCNET: www.sharcnet.ca) and Compute/Calcul Canada.

References

1 J. T. Vivian and P. R. Callis, *Biophysical Journal*, 2001, **80**, 2093–2109.
2 K. Cho, X. Wang, S. Nie, Z. Chen and D. M. Shin, *Clinical Cancer Research*, 2008, **14**, 1310–1316.
3 A. B. T. Ghisaidoobe and S. J. Chung, *International Journal of Molecular Sciences*, 2014, **15**, 22518–22538.
4 F. G. Graeff, F. S. Guimarães, T. G. C. S. De Andrade and J. F. W. Deakin, in *Pharmacology Biochemistry and Behavior*, 1996, vol. **54**, pp. 129–141.
5 J. Halford, J. Harrold, C. Lawton and J. Blundell, *Current Drug Targets*, 2012, **6**, 201–213.
6 B. H. Brummett, A. D. Krystal, A. Ashley-Koch, C. M. Kuhn, S. Züchner, I. C. Siegler, J. C. Barefoot, E. L. Ballard, L. P. Gwyther and R. B. Williams, *Psychosomatic Medicine*, 2007, **69**, 621–624.
7 N. Le Floc'h, W. Otten and E. Merlot, *Amino Acids*, 2011, **41**, 1195–1205.
8 T. W. Stone, *Pharmacological Reviews*, 1993, **45**, 309–379.
9 A. M. Myint, *FEBS Journal*, 2012, 279, 1375–1385.
10 L. J. Hu, X. F. Li, J. Q. Hu, X. J. Ni, H. Y. Lu, J. J. Wang, X. N. Huang, C. X. Lin, D. W. Shang and Y. G. Wen, *Journal of Analytical Toxicology*, 2017, **41**, 37–44.
11 D. Ungor, K. Horváth, I. Dékány and E. Csapó, *Sensors and Actuators, B: Chemical*, 2019, **288**, 728–733.
12 D. K. Hansen and S. M. Lunte, in *Journal of Chromatography A*, 1997, vol. 781, pp. 81–89.
13 M. Flint Beal, W. R. Matson, E. Storey, P. Milbury, E. A. Ryan, T. Ogawa and E. D. Bird, *Journal of the Neurological Sciences*, 1992, **108**, 80–87.
14 M. A. Yawer, V. Havel and V. Sindelar, *Angewandte Chemie - International Edition*, 2015, **54**, 276–279.
15 M. J. Langton, S. W. Robinson, I. Marques, V. Félix and P. D. Beer, *Nature Chemistry*, 2014, **6**, 1039–1043.
16 A. Borissov, I. Marques, J. Y. C. Lim, V. Félix, M. D. Smith and P. D. Beer, *Journal of the American Chemical Society*, 2019, **141**, 4119–4129.
17 N. G. White, S. Carvalho, V. Félix and P. D. Beer, *Organic and Biomolecular Chemistry*, 2012, **10**, 6951–6959.
18 X. Ji, R. T. Wu, L. Long, C. Guo, N. M. Khashab, F. Huang and J. L. Sessler, *Journal of the American Chemical Society*, 2018, **140**, 2777–2780.
19 K. Twum, J. M. Rautiainen, S. Yu, K. N. Truong, J. Feder, K. Rissanen, R. Puttreddy and N. K. Beyeh, *Crystal Growth and Design*, 2020, **20**, 2367–2376.
20 S. M. Taimoory, K. Twum, M. Dashti, F. Pan, M. Lahtinen, K. Rissanen, R. Puttreddy, J. F. Trant and N. K. Beyeh, *Journal of Organic Chemistry*, 2020, **85**, 5884–5894.
21 A. Velásquez-Silva, B. Cortés, Z. J. Rivera-Monroy, A. Pérez-Redondo and M. Maldonado, *Journal of Molecular Structure*, , DOI:10.1016/j.molstruc.2017.02.059.
22 R. Pinalli, E. Dalcanale, F. Ugozzoli and C. Massera, *CrystEngComm*, 2016, 18, 5788–5802.
23 S. Busi, H. Saxell, R. Fröhlich and K. Rissanen, *CrystEngComm*, 2008, **10**, 1803–1809.
24 N. K. Beyeh, A. Valkonen, S. Bhowmik, F. Pan and K. Rissanen, *Organic Chemistry Frontiers*, 2015, **2**, 340–345.
25 F. Davis, C. F. J. Faul and S. P. J. Higson, *Soft Matter*, 2009, **5**, 2746–2751.
26 H. Mansikkamäki, S. Busi, M. Nissinen, A. Åhman and K. Rissanen, *Chemistry - A European Journal*, 2006, **12**, 4289–4296.
27 B. Q. Ma and P. Coppens, *Crystal Growth and Design*, 2004, **4**, 1377–1385.
28 N. K. Beyeh, M. Kogej, A. Åhman, K. Rissanen and C. A. Schalley, *Angewandte Chemie - International Edition*, 2006, **45**, 5214–5218.
29 M. Vincenti and A. Irico, *International Journal of Mass Spectrometry*, 2002.
30 H. Mansikkamäki, M. Nissinen, C. A. Schalley and K. Rissanen, *New Journal of Chemistry*, 2003, **27**, 88–97.
31 N. K. Beyeh, I. Díez, S. M. Taimoory, D. Meister, A. I. Feig, J. F. Trant, R. H. A. Ras and K. Rissanen, *Chemical Science*, 2018, **9**, 1358–1367.
32 E. K. Kazakova, N. A. Makarova, A. U. Ziganshina, L. A. Muslinkina, A. A. Muslinkin and W. D. Habicher, *Tetrahedron Letters*, 2000, **41**, 10111–10115.
33 N. K. Beyeh, H. H. Jo, I. Kolesnichenko, F. Pan, E. Kalenius, E. V. Anslyn, R. H. A. Ras and K. Rissanen, *Journal of Organic Chemistry*, 2017, **82**, 5198–5203.
34 C. Schmidt, T. Straub, D. Falàbu, E. F. Paulus, E. Wegelius, E. Kolehmainen, V. Böhmer, K. Rissanen and W. Vogt, *European Journal of Organic Chemistry*, 2000, **2000**, 3937–3944.
35 A. Shivanyuk, T. P. Spaniol, K. Rissanen, E. Kolehmainen and V. Bohmer, *Angewandte Chemie - International Edition*, 2000, **39**, 3497–3500.
36 A. Shivanyuk and J. Rebek J., *Proceedings of the National Academy of Sciences of the United States of America*, 2001, **98**, 7662–7665.
37 J. S. Kim and D. T. Quang, *Chemical Reviews*, 2007, 107, 3780–3799.
38 M. J. Chaichi and S. O. Alijanpour, *Caspian J. Chem*, 2014, **3**, 15–21.
39 H. S. Geethanjali, D. Nagaraja, R. M. Melavanki and R. A. Kusanur, *Journal of Luminescence*, , DOI:10.1016/j.jlumin.2015.06.040.
40 M. V. Rusalov, S. I. Druzhinin and B. M. Uzhinov, in *Journal of Fluorescence*, 2004, vol. 14, pp. 193–202.
41 M. U. Kumke, H. G. Löhmannsröben and T. Roch, *Journal of Fluorescence*, , DOI:10.1007/BF00727531.
42 M. Teresa Montero, J. Hernández and J. Estelrich, *Biochemical Education*, 1990, **18**, 99–101.
43 M. W. Legenza, *Journal of Chemical Education*, 1977, **54**, 183–184.
44 B. Jeziorski, R. Moszynski and K. Szalewicz, *Chemical Reviews*, 2002, **94**, 1887–1930.

